



Published in final edited form as:

*Biochemistry*. 2012 July 24; 51(29): 5822–5830. doi:10.1021/bi300551b.

## UV resonance Raman monitors polyglutamine backbone and side chain hydrogen bonding and fibrillization<sup>1</sup>

Kan Xiong<sup>¶</sup>, David Punihaole, and Sanford A Asher

Department of Chemistry, University of Pittsburgh, Pittsburgh, PA 15260, Phone: (412)624-8570

Sanford A Asher: asher@pitt.edu

### Abstract

We utilize 198 and 204 nm excited UV resonance Raman spectroscopy (UVRR) and circular dichroism spectroscopy (CD) to monitor the backbone conformation and the GLN side chain hydrogen bonding (HB) of a short, mainly polyGLN peptide of sequence D<sub>2</sub>Q<sub>10</sub>K<sub>2</sub> (Q10). We measured the UVRR spectra of valeramide to determine the dependence of the primary amide vibrations on amide HB. We observe that non-disaggregated Q10 (NDQ10) solution (prepared by directly dissolving the original synthesized peptide in pure water) occurs in a  $\beta$ -sheet conformation, where the GLN side chains form HB to either the backbone or other GLN side chains. At 60 °C, these solutions readily form amyloid fibrils. We used the polyGLN disaggregation protocol of Wetzel et al (*Methods Enzymol*, **2006**, *413*, 34–74) to dissolve the Q10  $\beta$ -sheet aggregates. We observe that the disaggregated Q10 (DQ10) solutions adopt PPII-like and 2.5<sub>1</sub>-helix conformations where the GLN side chains form HB to water. In contrast, these samples do not form fibrils. The NDQ10  $\beta$ -sheet solution structure is essentially identical to that found in the NDQ10 solid formed upon solution evaporation. The DQ10 PPII and 2.5<sub>1</sub>-helix solution structure is essentially identical to that in the DQ10 solid. Although the NDQ10 solution readily forms fibrils when heated, the DQ10 solution does not form fibrils unless seeded by NDQ10 solution. This result demonstrates very high activation barriers between these solution conformations. The NDQ10 fibril secondary structure is essentially identical to that of the NDQ10 solution, except that the NDQ10 fibril backbone conformational distribution is narrower than in the dissolved species. The NDQ10 fibril GLN side chain geometry is more constrained than when NDQ10 is in solution. The NDQ10 fibril structure is identical to that of the DQ10 fibril seeded by the NDQ10 solution.

### Introduction

There are at least nine neurodegenerative diseases that are caused by long CAG DNA repeats that encode for proteins with long tracts of polyGLN residues. (1, 2) In these diseases, the extended polyGLN regions aggregate to form amyloid fibrils. (3–5) Previous studies suggest that polyGLN fibril structures are stabilized by both main chain and side chain HB. (6–9) However, there has been little work that investigates the role of HB in the aggregation mechanism(s) of polyGLN rich peptides and proteins. (10)

<sup>1</sup>This work was supported by NIH grant 1R01EB009089.

Correspondence to: Sanford A Asher, asher@pitt.edu.

<sup>¶</sup>Present address: Department of Chemistry, Northwestern University, Evanston, IL, 60208

#### Supporting Information

Methods for determination of  $\Psi$ -angle distributions from UVRR spectra; CD spectra of Q10 solutions by using different solvents for disaggregation. This information is available free of charge via the Internet at <http://pubs.acs.org/>.

Given the central role that backbone and side chain HB can potentially play in stabilizing polyGLN aggregates, it is important to find spectral markers for tracking these HB. Backbone HB is sometimes monitored by measuring the frequencies of the backbone amide vibrations, such as the AmI vibration (mainly C=O s) and the AmIII vibration (mainly in-phase combination of CN s and NH b) and the N-H stretching vibration. (11–16) The frequency of the AmII vibration (mainly out of phase combination of CN s and NH b) also depends on backbone HB. (17)

However, a method for studying side chain HB is needed. The C=O stretching frequencies of ASN, GLN, protonated ASP and GLU side chains are sensitive to HB. (18–20) Unfortunately, the use of IR spectroscopy for monitoring side chain vibrations is challenging due to spectral congestion, and isotopic labeling is often required to unambiguously assign bands. Solid state NMR spectroscopy (ssNMR) has been used to characterize GLN side chain HB. (21, 22) However, ssNMR requires long measurement times, and often requires sophisticated isotope labeling.

In this work here, we show that UVRR can selectively enhance the GLN primary amide side chain vibrations, and that these vibrations can be used to track GLN side chain HB. Here, we utilize 198 and 204 nm excited UVRR and CD to monitor the backbone conformation and the GLN side chain HB of a short, mainly polyGLN peptide Q10, of sequence D<sub>2</sub>Q<sub>10</sub>K<sub>2</sub>. Previous studies of similar peptides have shown that these peptides can aggregate to form  $\beta$ -sheet rich amyloid fibrils. (8, 9, 23–29) We observe that non-disaggregated Q10 (NDQ10) in solution occurs as  $\beta$ -sheets in which the GLN side chains form HB to either the backbone or other GLN side chains. At 60 °C, these solutions readily form amyloid fibrils. We used the polyGLN disaggregation protocol of Wetzel et al (30) to disaggregate Q10. We observe that disaggregated Q10 (DQ10) solution adopts PPII-like and 2.5<sub>1</sub>-helix conformations in which the GLN side chains form HB to water. These samples do not form fibrils. Addition of small quantities of NDQ10 readily nucleates fibrils. This directly demonstrates that high activation barrier occurs between the monomer extended DQ10 solution conformation and the  $\beta$ -sheet structures that fibrillize.

## Experimental Details

### Materials

The short mainly polyGLN peptide of sequence D<sub>2</sub>Q<sub>10</sub>K<sub>2</sub> (Q10) (> 90% purity) was synthesized by AnaSpec Inc, by using a solid phase peptide synthesis method. Briefly, the first amino acid Fmoc-AA-OH was coupled onto the resin and the peptide was synthesized through sequential synthetic operations of Fmoc deprotection, washing, Fmoc amino acid coupling, and washing. The synthesized crude peptide was obtained after acid cleavage from the solid support resin using a Trifluoroacetic acid (TFA) cocktail (where TFA is the major component).

The resulting crude peptide was then purified with preparative HPLC (using large columns and high flow rates) by using a mobile phase gradient consisting of 0.1 % (v/v) TFA in water and pure acetonitrile. The purified sample was then lyophilized.

Valeramide (97% purity) was purchased from Alfa Aesar. L-Glutamine (99% purity) was purchased from Acros. TFA (99.5% purity) was purchased from Acros. 1,1,1,3,3,3-hexafluoro-2-propanol (HFIP, 99% purity) was purchased from Fluka.

Solutions of non-disaggregated Q10 (NDQ10) were prepared by directly dissolving the peptide in pure water at 1 mg/ml concentrations at pH 4.3. NDQ10 solid samples were prepared by evaporating the NDQ10 solution. The UVRR spectra were identical to that of

the solid sample obtained from the manufacturer. We used the polyGLN disaggregation protocol of Wetzel et al (30) to dissolve the Q10 aggregates. Briefly, solutions of disaggregated Q10 (DQ10) were prepared by suspending 10 mg of Q10 in a 5 mL solution of 1:1 (v/v) TFA and HFIP [TFA alone dissolves Q10 aggregates (see Fig. S3 in supporting information); the primary function of HFIP is to facilitate the removal of TFA. (30)]. The samples were then sonicated for 20 min [Sonication is not essential (see Fig. S3 in supporting information)] and incubated at room temperature for ~ 2 hr. The solvents were evaporated with a gentle stream of dry N<sub>2</sub> gas for ~ 20 min. The peptide film was resuspended in pure water at a final concentration of ~ 1 mg/mL and the pH was adjusted to 7. The peptide solution was centrifuged at 627,000 g for 30 min at 4 °C, and the top 66% of the solution was used. DQ10 solid samples were prepared by evaporating the DQ10 solution. NDQ10 fibrils were prepared by incubating 4 mg/ml NDQ10 solution at 60 °C for ~ 1 week (60 °C was chosen to speed up the reaction). DQ10 fibrils were prepared by incubating 4 mg/ml DQ10 solution after seeding with 2 % NDQ10 solution at 60 °C for ~ 4 days. Fibrils were harvested by centrifugation at 627,000 g for 15 min.

CD spectra between 190 – 250 nm were measured by using a Jasco-715 spectropolarimeter with a 0.02 cm path length cuvette. Five 1-min accumulations were averaged.

The UVRR spectrometer was described in detail by Bykov et al. (31) Briefly, 204 nm UV light was obtained by generating the fifth anti-Stokes Raman harmonic of the third harmonic of a Nd:YAG laser (Coherent, Infinity). 198 nm UV light was obtained by mixing the 3<sup>rd</sup> harmonic of the 792 nm fundamental of a 1 KHz repetition rate tunable Ti:Sapphire laser (DM20-527 TU-L-FHG) from Photonics Industries.

The liquid sample was circulated in a free surface, temperature-controlled stream. A spinning cell was used for the solid samples to minimize photodegradation; the solid samples were packed into a circular groove of the cylindrical spinning disc. The fibrils were resuspended in 100 μL pure water and transferred into a spinning Suprasil NMR tube. A 165° sampling backscattering geometry was used. The collected light was dispersed by a double monochromator onto a back thinned CCD camera with a Lumogen E coating (Princeton Instruments-Spec 10 System). We averaged four 5-min accumulations. The Raman spectral frequencies are accurate to ± 1 cm<sup>-1</sup>. The relative standard deviations in spectral intensities are 1%.

Electron micrographs were measured by using a Tecnai T12 microscope (FEI) operating at 120 KV. Samples were prepared on carbon coated grids and stained with 2% uranyl acetate. Samples were magnified 30,000 X.

X ray patterns were measured by using a Bruker Smart Apex CCD diffractometer.

## Results

### UVRR of valeramide

We examined the UVRR spectra of valeramide in order to model the GLN side chain primary amide UVRR spectra, to determine the dependence of the primary amide vibrations on their HB to water. 198 and 204 nm excitation both occur within the  $\pi \rightarrow \pi^*$  electronic transition of the primary amide group.(32) Thus, the side chain amide group vibrations are selectively enhanced.

Fig. 1 shows the 204 nm excited UVRR spectra of valeramide in water at 22 °C and 65 °C. The 22 °C spectrum shows an AmI-like shoulder at ~ 1666 cm<sup>-1</sup> (mainly CO s) and an AmII-like band at 1606 cm<sup>-1</sup> (mainly NH<sub>2</sub> b with a small contribution from CO s). It also

shows a  $\delta_{\text{asCH}_3}$  shoulder at  $1458 \text{ cm}^{-1}$  (asymmetric deformation of the  $\text{CH}_3$  group), and a strong peak at  $1420 \text{ cm}^{-1}$  where the  $\delta_{\text{CH}_2}$  band ( $\text{CH}_2$  b) and an AmIII-like band (mainly CN s with minor contributions from  $\text{CH}_2$  b and  $\text{NH}_2$  r) overlap. The  $\omega_{\text{CH}_2}$  band occurs at  $1312 \text{ cm}^{-1}$  ( $\text{CH}_2$  w). The  $\nu_{\text{NH}_2}^1$  and  $\nu_{\text{NH}_2}^2$  bands (mainly  $\text{NH}_2$  r) occur at  $1132$  and  $1082 \text{ cm}^{-1}$ , respectively. (32–34)

As the temperature increases to  $65 \text{ }^\circ\text{C}$ , the AmI band frequency little changes. The AmII band upshifts  $2 \text{ cm}^{-1}$ . The  $\delta_{\text{asCH}_3}$  band downshifts  $2 \text{ cm}^{-1}$  and its intensity decreases. The AmIII+ $\delta_{\text{CH}_2}$  peak downshifts  $4 \text{ cm}^{-1}$ . The  $\omega_{\text{CH}_2}$  band does not change. The  $\nu_{\text{NH}_2}^1$  and  $\nu_{\text{NH}_2}^2$  bands both downshift  $2 \text{ cm}^{-1}$ .

**In acetonitrile**—The UVRR spectrum of valeramide in pure acetonitrile (Fig. 2) changes dramatically compared to that in pure water. The AmI band upshifts  $21 \text{ cm}^{-1}$  due to the decreased HB in acetonitrile, (17) and its relative intensity dramatically increases. The AmII band upshifts  $11 \text{ cm}^{-1}$  due to the decreased HB of the  $-\text{NH}_2$ . The frequency of the  $\delta_{\text{asCH}_3}$  band shows little change. The AmIII+ $\delta_{\text{CH}_2}$  peak and  $\omega_{\text{CH}_2}$  bands downshift  $31$  and  $12 \text{ cm}^{-1}$ , respectively. The  $\nu_{\text{NH}_2}^1$  and  $\nu_{\text{NH}_2}^2$  bands downshift  $6$  and  $16 \text{ cm}^{-1}$ , respectively.

**Solid state**—The UVRR spectrum of valeramide powder from the manufacturer (red, Fig. 3) differs significantly from that dissolved in water. The AmI band upshifts  $10 \text{ cm}^{-1}$ , indicative of weakened carbonyl HB, (17) and the relative intensity of the AmI band significantly increases. The AmII band downshifts  $5 \text{ cm}^{-1}$ . The AmIII+ $\delta_{\text{CH}_2}$  peak becomes asymmetric and upshifts  $12 \text{ cm}^{-1}$ . The  $\delta_{\text{asCH}_3}$  band is not evident. The frequency of  $\omega_{\text{CH}_2}$  band changes little. The  $\nu_{\text{NH}_2}^1$  and  $\nu_{\text{NH}_2}^2$  bands upshift  $10$  and  $8 \text{ cm}^{-1}$ , respectively.

### Raman cross sections for valeramide

We calculated the Raman cross sections for valeramide in water and in acetonitrile by using eq 1:(35)

$$\sigma_{\text{val}} = \frac{I_{\text{val}} \cdot k(\lambda_r) \cdot C_r \cdot \sigma_r}{I_r \cdot k(\lambda_{\text{val}}) \cdot C_{\text{val}}} \cdot \left[ \frac{\epsilon_{\text{val}} + \epsilon_{\text{ex}}}{\epsilon_r + \epsilon_{\text{ex}}} \right] \quad \text{eqn 1}$$

where  $I_{\text{val}}$  and  $I_r$  are the relative intensities of the valeramide band and the internal standard band (which is the  $932 \text{ cm}^{-1}$   $\text{ClO}_4^-$  band in aqueous solution or the  $918 \text{ cm}^{-1}$  C-C stretching band of acetonitrile in pure acetonitrile(36)).  $k(\lambda_r)$  and  $k(\lambda_{\text{val}})$  are the spectrometer efficiencies at the wavelengths of the internal standard and valeramide Raman bands.  $C_r$  and  $C_{\text{val}}$  are the concentrations of the internal standard and valeramide, respectively.  $\sigma_r$  is the total differential Raman cross section of the internal standard band at the excitation frequency,  $\nu_{\text{ex}}$ .  $\epsilon_{\text{ex}}$  is the sample molar absorptivity at  $\nu_{\text{ex}}$ .  $\epsilon_{\text{val}}$  and  $\epsilon_r$  are the sample molar absorptivities at the valeramide Raman band frequency and the internal standard band frequency, respectively. The expression in the brackets approximately corrects the Raman intensities for self-absorption in a backscattering geometry.

Table 1 shows the measured total differential Raman cross sections for valeramide. The  $204 \text{ nm}$  Raman cross section values of the valeramide amide bands in pure water are approximately half of those of protein backbone secondary amide bands, (37) presumably because the primary amide group electronic transition is blueshifted from that of the peptide bond secondary amides. (32)

The Raman cross sections of the valeramide bands in pure acetonitrile are decreased relative to those in pure water, except for the AmI band cross section, that doubles. A similar behavior was observed for the AmI band of N-methylacetamide. (38) The increased cross

section was ascribed to a larger relative CO bond excited state displacement in acetonitrile. (38) The Raman cross sections of the valeramide bands generally triple as the excitation wavelength decreases from 204 to 198 nm, except for the AmII band cross section in acetonitrile, that increases by more than 10-fold. The 198 nm Raman cross section values of the valeramide primary amide bands are similar to those of the protein backbone secondary amide bands. (37)

### Hydrogen bonding effects on frequencies of primary amide vibrations

These UVRR studies of valeramide indicate that the AmI, AmII,  $\nu\text{NH}_2^1$  and  $\nu\text{NH}_2^2$  frequencies of the primary amide depend on HB. Water HB to the carbonyls downshifts the AmI band by  $21\text{ cm}^{-1}$  (see Table 2), while HB to the  $-\text{NH}_2$  upshifts the  $\nu\text{NH}_2^1$  and  $\nu\text{NH}_2^2$  bands by  $6$  and  $16\text{ cm}^{-1}$ , respectively; the AmII band downshifts  $11\text{ cm}^{-1}$  upon HB to  $-\text{NH}_2$ . The solid state AmI band upshifts  $10\text{ cm}^{-1}$  relative to that in water, indicating weaker carbonyl HB in the valeramide solid than in water. The solid state AmII band downshifts  $7\text{ cm}^{-1}$  compared to that in water, and the  $\nu\text{NH}_2^1$  and  $\nu\text{NH}_2^2$  bands upshift  $12$  and  $10\text{ cm}^{-1}$ , respectively. This indicates stronger  $-\text{NH}_2$  HB in the valeramide solid than in water.

X ray studies of butyramide solid (39) (which has one less methylene than valeramide) indicate that each carbonyl forms two HBs to the two amine H atoms of two adjacent molecules, while each  $-\text{NH}_2$  forms two HBs to two carbonyls. This stronger  $-\text{NH}_2$  HB may result from the fact that while the valeramide carbonyl HB geometry is more optimized in water than in the solid state, the  $-\text{NH}_2$  HB is stronger in the solid state.

### Q10 solution backbone conformation

We performed both CD and UVRR measurements to examine the Q10 solution backbone conformation. Previous studies of similar peptides indicate that non-disaggregated polyGLN peptides in aqueous solutions occur as  $\beta$ -sheets, (24) while freshly disaggregated polyGLN peptides adopt extended conformations. (40, 41)

Fig. 4 shows the CD spectra of Q10 solutions. The CD spectrum of the NDQ10 in pure water (dashed line) shows a trough at  $\sim 218\text{ nm}$  and a strong positive band at  $197\text{ nm}$ , both characteristic of  $\beta$ -sheet. (42) The spectrum of the DQ10 in pure water (solid line) shows a very slight negative ellipticity at  $\sim 220\text{ nm}$  and a strong negative band at  $200\text{ nm}$ , indicative of extended conformations. (43–45)

$204\text{ nm}$  excitation occurs within the  $\pi \rightarrow \pi^*$  electronic transition of the backbone secondary amides (37) and to the long wavelength side of the side chain primary amide electronic transitions. (32) Fig. 5 shows that the  $204\text{ nm}$  excited UVRR spectra of Q10 solutions are dominated by the backbone amide vibrations (indicated by <sup>b</sup>). The backbone amide vibrations are more enhanced by  $204\text{ nm}$  excitation than are those of the side chain amide (indicated by <sup>s</sup>; the side chain amide bands were assigned based on the measured valeramide primary amide band frequencies). (32)

The UVRR spectrum of the NDQ10 (red) shows an AmI<sup>b</sup> band at  $\sim 1660\text{ cm}^{-1}$ , an AmII<sup>b</sup> band at  $\sim 1550\text{ cm}^{-1}$ , the  $(\text{C})\text{C}_\alpha\text{-H}^b$  bending bands at  $\sim 1400\text{ cm}^{-1}$ , and the AmIII<sup>b</sup> region between  $1180$  and  $1330\text{ cm}^{-1}$ . The AmI<sup>b</sup> band overlaps with the GLN side chain AmI<sup>s</sup> band; the  $\text{C}_\alpha\text{H}^b$  band overlaps with the side chain AmIII<sup>s</sup>+ $\delta_{\text{CH}_2}$  peak.

The AmIII<sup>b</sup> region of Q10 contains no overlapping side chain contributions. We calculated the Ramachandran  $\Psi$  probability distributions for the Q10 backbone peptide bonds from the Fig. 5 UVRR spectra by using the methodology of Mikhonin et al (11, 46, 47). This method correlates different AmIII<sub>3</sub> frequencies of the band envelope to different peptide bond  $\Psi$  angles. This deconvolutes the inhomogeneously broadened AmIII bandshape to a  $\Psi$  angle

distribution (see supporting information for details). The estimated error of this Ramachandran  $\Psi$  angle determination was suggested to be  $\pm 14^\circ$ . (11)

The Fig. 6  $\Psi$ -distribution for the NDQ10 shows a dominant  $\beta$ -sheet contribution ( $\Psi \sim 138^\circ$ ). It also contains contributions from Type I, Type III or Type VIII  $\beta$ -turn regions ( $\Psi \sim -40^\circ$ ). The  $\Psi$ -distribution for the DQ10 shows a dominant contribution of PPII-like ( $\Psi \sim 145^\circ$ ) and  $2.5_1$ -helix conformations ( $\Psi \sim 170^\circ$ ). It also contains contributions of Type I' or Type III'  $\beta$ -turns ( $\Psi \sim 30^\circ$ ).

Previous studies indicate that poly-L-lysine and poly-L-glutamate adopt  $2.5_1$ -helix conformations that are stabilized by electrostatic repulsion between the charged side chains. (48–50) We surprisingly find that DQ10 adopts  $2.5_1$ -helix conformations. The mechanism(s) by which these  $2.5_1$ -helix conformations of Q10 are stabilized is unknown.

### Q10 solution side chain hydrogen bonding

198 nm excitation (Fig. 7) enhances the primary amide UVRR bands significantly more than does 204 nm excitation. As a result, the difference spectrum between the 198 and 204 nm excited UVRR spectra of Q10 (Fig. 7) is dominated by the GLN side chain primary amide bands.

The 198 – 204 nm difference spectrum of NDQ10 in pure water (Fig. 8) shows an AmI<sup>s</sup> band at  $1657\text{ cm}^{-1}$  and an AmII<sup>s</sup> band at  $1614\text{ cm}^{-1}$ . It also shows an AmIII<sup>s</sup> band at  $1414\text{ cm}^{-1}$  and a  $\omega_{\text{CH}_2}$  band at  $1353\text{ cm}^{-1}$ . The  $\nu\text{NH}_2^1$  and  $\nu\text{NH}_2^2$  bands occur at  $1110$  and  $1056\text{ cm}^{-1}$ , respectively.

The 198 – 204 nm difference spectrum of DQ10 in pure water (Fig. 8, black) differs significantly from that of NDQ10. The DQ10 AmI<sup>s</sup> band upshifts  $26\text{ cm}^{-1}$ , indicating weaker HB of the GLN side chain carbonyls than that of NDQ10. The AmII<sup>s</sup> frequency shows little change. The AmIII<sup>s</sup> frequency upshifts  $22\text{ cm}^{-1}$ . The DQ10  $\nu\text{NH}_2^1$  and  $\nu\text{NH}_2^2$  frequencies upshift  $13$  and  $19\text{ cm}^{-1}$  respectively, indicating stronger HB of the GLN side chain  $-\text{NH}_2$  than in NDQ10.

The frequencies of the GLN primary amide vibrations of the DQ10 in pure water (Fig. 8, black) are very similar to those of glutamine in pure water (Fig. 8, blue); the 204 nm excited UVRR spectrum of glutamine only contains side chain amide vibrations, there are no secondary amides. This indicates that HB of the GLN side chains of DQ10 is similar to that of glutamine in pure water; i.e., the GLN side chains of DQ10 form HB to water.

The DQ10 AmIII<sup>s</sup> band significantly narrows compared to glutamine in water. This may result from the fact that the glutamine side chain has conformations in solution where the primary amide side chain interacts with the  $-\text{NH}_3^+$  groups.

Previous studies indicated that polyGLN aggregates adopt  $\beta$ -sheet conformations that are stabilized by both main chain and side chain HB. (6–9) We observe that the GLN side chain HB of NDQ10 differs significantly from that of DQ10. The NDQ10 AmI<sup>s</sup> frequency downshifts  $26\text{ cm}^{-1}$  relative to that of DQ10, and its  $\nu\text{NH}_2^1$  and  $\nu\text{NH}_2^2$  frequencies downshift  $13$  and  $19\text{ cm}^{-1}$  respectively. Table 2 shows that HB to the primary amide carbonyls significantly downshift the AmI<sup>s</sup> frequency, while HB to the  $-\text{NH}_2$  upshift the  $\nu\text{NH}_2^1$  and  $\nu\text{NH}_2^2$  frequencies. Thus, HB of the NDQ10 GLN side chain carbonyls is stronger than that of DQ10, while HB of its GLN side chain  $-\text{NH}_2$  is weaker than that of DQ10. These results indicate that the GLN side chain carbonyls of NDQ10 do not form HB to water. Instead, they form HB to the backbone  $-\text{NH}$  or to GLN side chain  $-\text{NH}_2$ . Presumably, this conformation results in weaker  $-\text{NH}_2$  HB.

## Q10 solids

We measured the 204 nm excited UVRR spectra of Q10 solids formed by evaporation of the NDQ10 and DQ10 solutions. The UVRR spectral frequencies of the NDQ10 solid (Fig. 9, black) are very similar to that of NDQ10 in solution (Fig. 9, red), indicating that the backbone conformations and the GLN side chain HB of NDQ10 solid and solution are essentially identical, and mainly  $\beta$ -sheet. The NDQ10 solid shows a powder X ray pattern (Fig. 10) very similar to that of Perutz et al.(23) The 4.75-Å reflection (Fig. 10) is characteristic of  $\beta$ -sheet structures.(23)

The AmIII<sup>b</sup> region of the solvent evaporated DQ10 solid (Fig. 9, blue) is similar to that of DQ10 solution (Fig. 9, green), indicating that their Q10 backbone conformations are similar. The solid state AmII<sup>b</sup> band downshifts 7 cm<sup>-1</sup> compared to that of solution, indicating weakened HB of the solid state backbone -NH(17); while the solid state AmI<sup>b</sup> and AmI<sup>s</sup> bands upshift 5 cm<sup>-1</sup> relative to that of solution, indicating weakened HB to the solid backbone carbonyls and the GLN side chain carbonyls. (17)

These results indicate the Q10 solution and solid state conformations are essentially identical.

This suggests that the solution state activation barriers between extended PPII and 2.5<sub>1</sub>-helix conformations and the  $\beta$ -sheet aggregate conformations are very high; these structures are not in an equilibrium in solution or during solution evaporation.

## Q10 solution fibrillization

We observe that NDQ10 in pure water forms amyloid fibrils after incubation at 60 °C for ~ 2 days (confirmed by using TEM and the ThT binding assay (24); the short time TEM of NDQ10 does not show fibril structures, see Fig. S4 in supporting information). In contrast, DQ10 does not form fibrils even after incubation for > 2 weeks at 60 °C. However, upon seeding with a small aliquot of the NDQ10 solution, the DQ10 solution readily forms fibrils at 60 °C (confirmed by using TEM and the ThT binding assay). Thus, NDQ10 appears to contain small aggregates that seed fibrillation.

Thus, the activation barrier for DQ10 to form  $\beta$ -sheet aggregates that evolve to NDQ10 fibrils is quite high. The fact that DQ10 solutions do not self nucleate fibrils is consistent with previous studies of similar peptides. (24, 51, 52)

## Q10 fibrils

Fig. 11a and b show electron micrographs of the NDQ10 fibrils, and the DQ10 fibrils formed upon seeding with the NDQ10 solution. Fig. 11c shows the 204 nm excited UVRR spectra of the NDQ10 fibrils, the DQ10 fibrils and the UVRR spectrum of the NDQ10 solution. The NDQ10 fibril band frequencies (Fig. 11c, red) are very similar to those of the NDQ10 solution (Fig. 11c, black). Thus, the NDQ10 fibrils also occur in a  $\beta$ -sheet structure in which the GLN side chains form HB to the backbone or to other GLN side chains. However, the NDQ10 fibril bands are significantly narrowed compared to those in the NDQ10 solution, indicating a narrower backbone conformational distribution and more constrained GLN side chain geometries for the NDQ10 fibrils than for the NDQ10 solution.

The UVRR spectrum of the DQ10 fibrils formed upon seeding with an aliquot of the NDQ10 solution (Figure 11c, blue) is identical to that of the NDQ10 fibrils spontaneously formed (Figure 11c, red), indicating identical Q10 backbone conformations and GLN side chain HB.

## Discussion

### Q10 Structure

CD and UVRR studies indicate that NDQ10 in pure water adopts a predominantly  $\beta$ -sheet structure, consistent with previous studies indicating that polyGLN aggregates form  $\beta$ -sheet rich structures. (24, 53) UVRR also observes turn conformations in NDQ10. The fractions of  $\beta$ -sheet and turn conformations are 0.84 and 0.16, respectively. This ratio suggests that NDQ10 in pure water occurs as  $\beta$ -hairpins in which two residues are in the turn region and eleven residues form a  $\beta$ -sheet structure (Fig. 12).

We observe that DQ10 in pure water adopts predominantly PPII-like and  $2.5_1$ -helix conformations (Fig. 12). Previous studies indicate that glutamine residues in short polyGLN sequences have a high propensity to form PPII-like conformations,(40, 41) other studies, however, report disordered structures.(29, 51, 54–57)

198 and 204 nm excited UVRR indicate that the GLN side chains of NDQ10 form HB to the backbone or other GLN side chains, while the GLN side chains of DQ10 form HB to water.

We also observe that the NDQ10 fibril secondary structure is essentially identical to that in the NDQ10 solution, except that the NDQ10 fibril backbone conformational distribution is narrower. Thus, the fibril GLN side chain geometry is more constrained than that of the NDQ10 solution.

The UVRR determined NDQ10 fibril structure appears identical to that of the DQ10 fibrils seeded by an aliquot of the NDQ10 solution. These results suggest that the Q10 fibrils consist of stacks of  $\beta$ -hairpins. Previous studies of a similar peptide of sequence  $D_2Q_{15}K_2$  also indicated  $\beta$ -hairpin fibril structure. (8, 9, 25)

## Conclusions

We utilize UVRR and CD to monitor the backbone conformation and the GLN side chain HB of a short mainly polyGLN peptide Q10, of sequence  $D_2Q_{10}K_2$ . We measured UVRR spectra of valeramide to determine the dependence of primary amide vibrations on the primary amide HB. We observe that NDQ10 occurs in a  $\beta$ -sheet-like structure in which the GLN side chains form HB to the backbone or other GLN side chains.

These solutions readily form amyloid fibrils. In contrast, DQ10 solutions adopt PPII-like and  $2.5_1$ -helix conformations in which the GLN side chains form HB to water. These samples do not form fibrils upon heating within two weeks. The NDQ10 and DQ10 solution structures are essentially identical to their solid state structures. Although the NDQ10 solution readily forms fibrils when heated, the DQ10 solution does not form fibrils unless seeds from the NDQ10 solution are added. This indicates very high activation barriers occur between these solution conformations.

The Q10 fibril secondary structure is essentially identical to that of the NDQ10 solution, except that the fibril backbone conformational distribution is narrower and its GLN side chain geometry is more constrained compared to that of the NDQ10 solution.

## Supplementary Material

Refer to Web version on PubMed Central for supplementary material.

## Acknowledgments

We thank Dr. Sergei V. Bykov for useful discussions. We also thank Lu Ma for help with instrumentation.

## References

1. Zoghbi HY, Cummings CJ. Fourteen and counting: unraveling trinucleotide repeat diseases. *Hum Mol Genet.* 2000; 9:909–916. [PubMed: 10767314]
2. Ross CA, Poirier MA. What is the role of protein aggregation in neurodegeneration? *Nat Rev Mol Cell Biol.* 2005; 6:891–898. [PubMed: 16167052]
3. Wetzel R, Bhattacharyya AM, Thakur AK. Polyglutamine aggregation nucleation: Thermodynamics of a highly unfavorable protein folding reaction. *Proc Natl Acad Sci USA.* 2005; 102:15400–15405. [PubMed: 16230628]
4. Wetzel R, Chen SM, Ferrone FA. Huntington's disease age-of-onset linked to polyglutamine aggregation nucleation. *Proc Natl Acad Sci USA.* 2002; 99:11884–11889. [PubMed: 12186976]
5. Wetzel R, Slepko N, Bhattacharyya AM, Jackson GR, Steffan JS, Marsh JL, Thompson LM. Normal-repeat-length polyglutamine peptides accelerate aggregation nucleation and cytotoxicity of expanded polyglutamine proteins. *Proc Natl Acad Sci USA.* 2006; 103:14367–14372. [PubMed: 16980414]
6. Rossetti G, Magistrato A, Pastore A, Persichetti F, Carloni P. Structural Properties of Polyglutamine Aggregates Investigated via Molecular Dynamics Simulations. *J Phys Chem B.* 2008; 112:16843–16850. [PubMed: 19367817]
7. Smith MH, Miles TF, Sheehan M, Alfieri KN, Kokona B, Fairman R. Polyglutamine fibrils are formed using a simple designed beta-hairpin model. *Proteins-Struct, Func, Bioinform.* 2010; 78:1971–1979.
8. Perutz MF, Johnson T, Suzuki M, Finch JT. Glutamine repeats as polar zippers: their possible role in inherited neurodegenerative diseases. *Proc Natl Acad Sci USA.* 1994; 91:5355–5358.
9. Sikorski P, Atkins E. New model for crystalline polyglutamine assemblies and their connection with amyloid fibrils. *Biomacromolecules.* 2005; 6:425–432. [PubMed: 15638548]
10. Nagai Y, Inui T, Popiel HA, Fujikake N, Hasegawa K, Urade Y, Goto Y, Naiki H, Toda T. A toxic monomeric conformer of the polyglutamine protein. *Nat Struct Mol Biol.* 2007; 14:332–340. [PubMed: 17369839]
11. Mikhonin AV, Bykov SV, Myshakina NS, Asher SA. Peptide secondary structure folding reaction coordinate: Correlation between UV Raman amide III frequency, Psi Ramachandran angle, and hydrogen bonding. *J Phys Chem B.* 2006; 110:1928–1943. [PubMed: 16471764]
12. Manas ES, Getahun Z, Wright WW, DeGrado WF, Vanderkooi JM. Infrared spectra of amide groups in alpha-helical proteins: Evidence for hydrogen bonding between helices and water. *J Am Chem Soc.* 2000; 122:9883–9890.
13. Wang Y, Purrello R, Jordan T, Spiro TG. UVRR spectroscopy of the peptide bond. 1. Amide S, a nonhelical structure marker, is a C $\alpha$ H bending mode. *J Am Chem Soc.* 1991; 113:6359–6368.
14. Mirkin NG, Krimm S. Structural dependence of NH stretch mode frequency shifts in amide and peptide. *J Phys Chem A.* 2004; 108:5438–5448.
15. Fu L, Liu J, Yan ECY. Chiral Sum Frequency Generation Spectroscopy for Characterizing Protein Secondary Structures at Interfaces. *J Am Chem Soc.* 2011; 133:8094–8097. [PubMed: 21534603]
16. Fu L, Wang Z, Yan EC. Chiral vibrational structures of proteins at interfaces probed by sum frequency generation spectroscopy. *Int J Mol Sci.* 2011; 12:9404–9425. [PubMed: 22272140]
17. Myshakina NS, Ahmed Z, Asher SA. Dependence of amide vibrations on hydrogen bonding. *J Phys Chem B.* 2008; 112:11873–11877. [PubMed: 18754632]
18. Barth A. The infrared absorption of amino acid side chains. *Prog Biophys Mol Biol.* 2000; 74:141–173. [PubMed: 11226511]
19. Takei K, Takahashi R, Noguchi T. Correlation between the hydrogen-bond structures and the C=O stretching frequencies of carboxylic acids as studied by density functional theory calculations: Theoretical basis for interpretation of infrared bands of carboxylic groups in proteins. *J Phys Chem B.* 2008; 112:6725–6731. [PubMed: 18452327]

20. Natalello A, Frana AM, Relini A, Apicella A, Invernizzi G, Casari C, Gliozzi A, Doglia SM, Tortora P, Regonesi ME. A Major Role for Side-Chain Polyglutamine Hydrogen Bonding in Irreversible Ataxin-3 Aggregation. *Plos One*. 2011; 6:e18789. [PubMed: 21533208]
21. Schneider R, Schumacher MC, Mueller H, Nand D, Klaukien V, Heise H, Riedel D, Wolf G, Behrmann E, Raunser S, Seidel R, Engelhard M, Baldus M. Structural characterization of polyglutamine fibrils by solid-state NMR spectroscopy. *J Mol Biol*. 2011; 412:121–136. [PubMed: 21763317]
22. Sivanandam VN, Jayaraman M, Hoop CL, Kodali R, Wetzel R, van der Wel PC. The aggregation-enhancing huntingtin N-terminus is helical in amyloid fibrils. *J Am Chem Soc*. 2011; 133:4558–4566. [PubMed: 21381744]
23. Perutz MF, Finch JT, Berriman J, Lesk A. Amyloid fibers are water-filled nanotubes. *Proc Natl Acad Sci USA*. 2002; 99:5591–5595.
24. Chen SM, Berthelie V, Hamilton JB, O’Nuallain B, Wetzel R. Amyloid-like features of polyglutamine aggregates and their assembly kinetics. *Biochemistry*. 2002; 41:7391–7399. [PubMed: 12044172]
25. Sharma D, Shinchuk LM, Inouye H, Wetzel R, Kirschner DA. Polyglutamine homopolymers having 8–45 residues form slablike beta-crystallite assemblies. *Proteins-Struct, Func, Bioinform*. 2005; 61:398–411.
26. Lee CC, Walters RH, Murphy RM. Reconsidering the mechanism of polyglutamine peptide aggregation. *Biochemistry*. 2007; 46:12810–12820. [PubMed: 17929830]
27. Darnell G, Orgel JPRO, Pahl R, Meredith SC. Flanking polyproline sequences inhibit beta-sheet structure in polyglutamine segments by inducing PPII-like helix structure. *J Mol Biol*. 2007; 374:688–704. [PubMed: 17945257]
28. Kar K, Jayaraman M, Sahoo B, Kodali R, Wetzel R. Critical nucleus size for disease-related polyglutamine aggregation is repeat-length dependent. *Nat Struct Mol Biol*. 2011; 18:328–336. [PubMed: 21317897]
29. Walters RH, Murphy RM. Examining Polyglutamine Peptide Length: A Connection between Collapsed Conformations and Increased Aggregation. *J Mol Biol*. 2009; 393:978–992. [PubMed: 19699209]
30. O’Nuallain B, Thakur AK, Williams AD, Bhattacharyya AM, Chen SM, Thiagarajan G, Wetzel R. Kinetics and thermodynamics of amyloid assembly using a high-performance liquid chromatography-based sedimentation assay. *Methods Enzymol*. 2006; 413:34–74. [PubMed: 17046390]
31. Bykov S, Lednev I, Ianoul A, Mikhonin A, Munro C, Asher SA. Steady-state and transient ultraviolet resonance Raman spectrometer for the 193–270 nm spectral region. *Appl Spectrosc*. 2005; 59:1541–1552. [PubMed: 16390595]
32. Dudik JM, Johnson CR, Asher SA. Uv Resonance Raman Studies of Acetone, Acetamide, and N-Methylacetamide - Models for the Peptide-Bond. *J Phys Chem*. 1985; 89:3805–3814.
33. Kuroda Y, Saito Y, Uno T, Machida K. Vibrational-Spectra of Propionamide and Its C-Deuterated and N-Deuterated Compounds. *Bull Chem Soc Jap*. 1972; 45:2371–2383.
34. Nandini G, Sathyanarayana DN. Ab initio studies on molecular conformation and vibrational spectra of propionamide. *J Mol Struct-Theochem*. 2002; 586:125–135.
35. Xiong K, Asher SA. Lowest Energy Electronic Transition in Aqueous Cl<sup>-</sup> Salts: Cl<sup>-</sup> → (H<sub>2</sub>O)<sub>6</sub> Charge Transfer Transition. *J Phys Chem A*. 2011; 115:9345–9348. [PubMed: 21105675]
36. Dudik JM, Johnson CR, Asher SA. Wavelength Dependence of the Preresonance Raman Cross-Sections of CH<sub>3</sub>CN, SO<sub>4</sub><sup>2-</sup>, ClO<sub>4</sub><sup>-</sup>, and NO<sub>3</sub><sup>-</sup>. *J Chem Phys*. 1985; 82:1732–1740.
37. Sharma B, Bykov SV, Asher SA. UV resonance Raman investigation of electronic transitions in alpha-helical and polyproline II-like conformations. *J Phys Chem B*. 2008; 112:11762–11769. [PubMed: 18712913]
38. Chen XG, Asher SA, Schweitzerstenner R, Mirkin NG, Krimm S. UV Raman Determination of the π – π\* Excited-State Geometry of N-Methylacetamide - Vibrational Enhancement Pattern. *J Am Chem Soc*. 1995; 117:2884–2895.
39. Lewis TC, Tocher DA. A low-temperature determination of butyramide. *Acta Crystal Sec E-Struct Reports Online*. 2005; 61:O1985–O1986.

40. Chellgren BW, Miller AF, Creamer TP. Evidence for polyproline II helical structure in short polyglutamine tracts. *J Mol Biol.* 2006; 361:362–371. [PubMed: 16854433]
41. Wang XL, Vitalis A, Wyczalkowski MA, Pappu RV. Characterizing the conformational ensemble of monomeric polyglutamine. *Proteins-Struct, Func, Bioinform.* 2006; 63:297–311.
42. Woody, RW. *Theory of Circular Dichroism of Proteins.* Plenum Press; New York: 1996.
43. Sreerama N, Woody RW. Poly(Pro)II Helices in Globular-Proteins - Identification and Circular Dichroic Analysis. *Biochemistry.* 1994; 33:10022–10025. [PubMed: 8060970]
44. Shi Z, Olson C, Rose G, Baldwin R, Kallenbach N. Polyproline II structure in a sequence of seven alanine residues. *Proc Natl Acad Sci USA.* 2002; 99:9190–9195. [PubMed: 12091708]
45. Shi Z, Chen K, Liu Z, Kallenbach N. Conformation of the backbone in unfolded proteins. *Chem Rev.* 2006; 106:1877–1897. [PubMed: 16683759]
46. Mikhonin AV, Asher SA. Direct UV Raman monitoring of  $3_{10}$ -helix and  $\pi$ -bulge premelting during alpha-helix unfolding. *J Am Chem Soc.* 2006; 128:13789–13795. [PubMed: 17044707]
47. Asher SA, Mikhonin AV, Bykov S. UV Raman demonstrates that alpha-helical polyalanine peptides melt to polyproline II conformations. *J Am Chem Soc.* 2004; 126:8433–8440. [PubMed: 15238000]
48. Mikhonin AV, Myshakina NS, Bykov SV, Asher SA. UV resonance Raman determination of polyproline II, extended  $2.5_1$ -helix, and beta-sheet psi angle energy landscape in poly-L-lysine and poly-L-glutamic acid. *J Am Chem Soc.* 2005; 127:7712–7720. [PubMed: 15913361]
49. Ma L, Ahmed Z, Asher SA. Ultraviolet Resonance Raman Study of Side Chain Electrostatic Control of Poly-L-Lysine Conformation. *J Phys Chem B.* 2011; 115:4251–4258. [PubMed: 21413713]
50. Xiong K, Ma L, Asher SA. Conformation of poly-L-glutamate is independent of ionic strength. *Biophys Chem.* 2012; 162:1–5. [PubMed: 22236769]
51. Chen S, Berthelie V, Yang W, Wetzel R. Polyglutamine aggregation behavior in vitro supports a recruitment mechanism of cytotoxicity. *J Mol Biol.* 2001; 311:173–182. [PubMed: 11469866]
52. Chen S, Wetzel R. Solubilization and disaggregation of polyglutamine peptides. *Protein Sci.* 2001; 10:887–891. [PubMed: 11274480]
53. Sharma D, Sharma S, Pasha S, Brahmachari SK. Peptide models for inherited neurodegenerative disorders: conformation and aggregation properties of long polyglutamine peptides with and without interruptions. *FEBS Lett.* 1999; 456:181–185. [PubMed: 10452554]
54. Chen SM, Ferrone FA, Wetzel R. Huntington's disease age-of-onset linked to polyglutamine aggregation nucleation. *Proc Natl Acad Sci USA.* 2002; 99:11884–11889. [PubMed: 12186976]
55. Crick SL, Jayaraman M, Frieden C, Wetzel R, Pappu RV. Fluorescence correlation spectroscopy shows that monomeric polyglutamine molecules form collapsed structures in aqueous solutions. *Proc Natl Acad Sci USA.* 2006; 103:16764–16769. [PubMed: 17075061]
56. Masino L, Kelly G, Leonard K, Trottier Y, Pastore A. Solution structure of polyglutamine tracts in GST-polyglutamine fusion proteins. *Febs Letters.* 2002; 513:267–272. [PubMed: 11904162]
57. Walters RH, Murphy RM. Examining polyglutamine peptide length: a connection between collapsed conformations and increased aggregation. *J Mol Biol.* 2009; 393:978–992. [PubMed: 19699209]

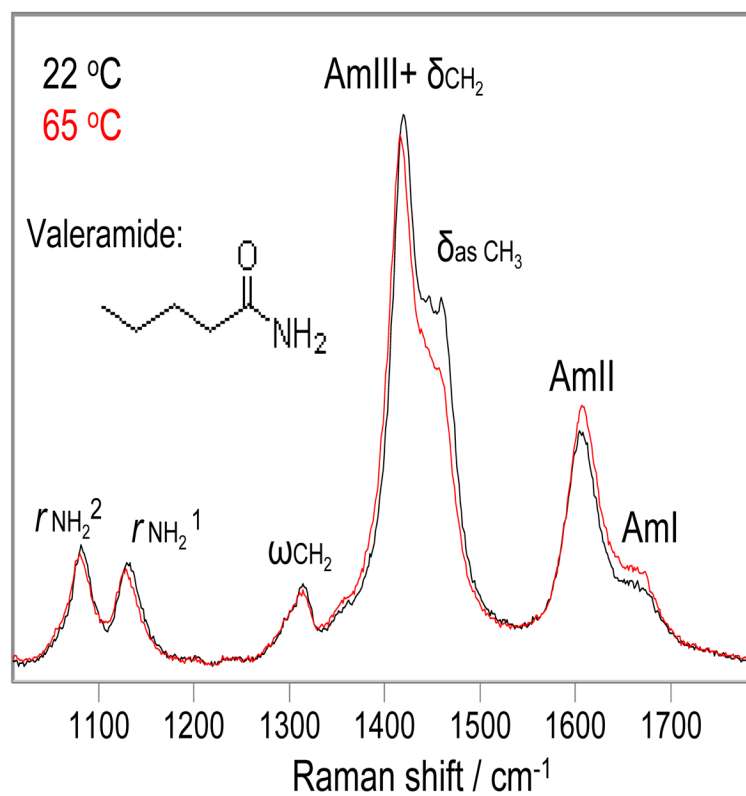


**Figure 1.** Temperature dependence of the 204 nm excited UVRR spectra of valeramide in water at 22 °C (**Black**) and 65 °C (**Red**). Water contributions were removed. The intensities were normalized to the  $932 \text{ cm}^{-1}$   $\text{ClO}_4^-$  peak height.

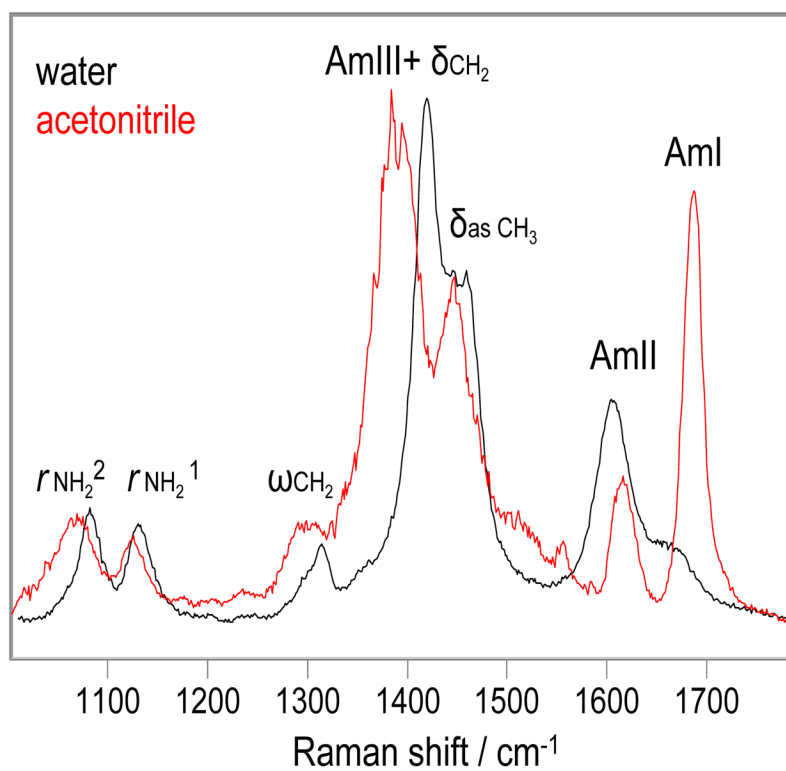


**Figure 2.** The 204 nm excited UVRR spectra of valeramide at 22 °C: **Black** in water; **Red** in pure acetonitrile. Solvent contributions were removed. The intensities were normalized to the AmIII+ $\delta$ CH<sub>2</sub> peak height.

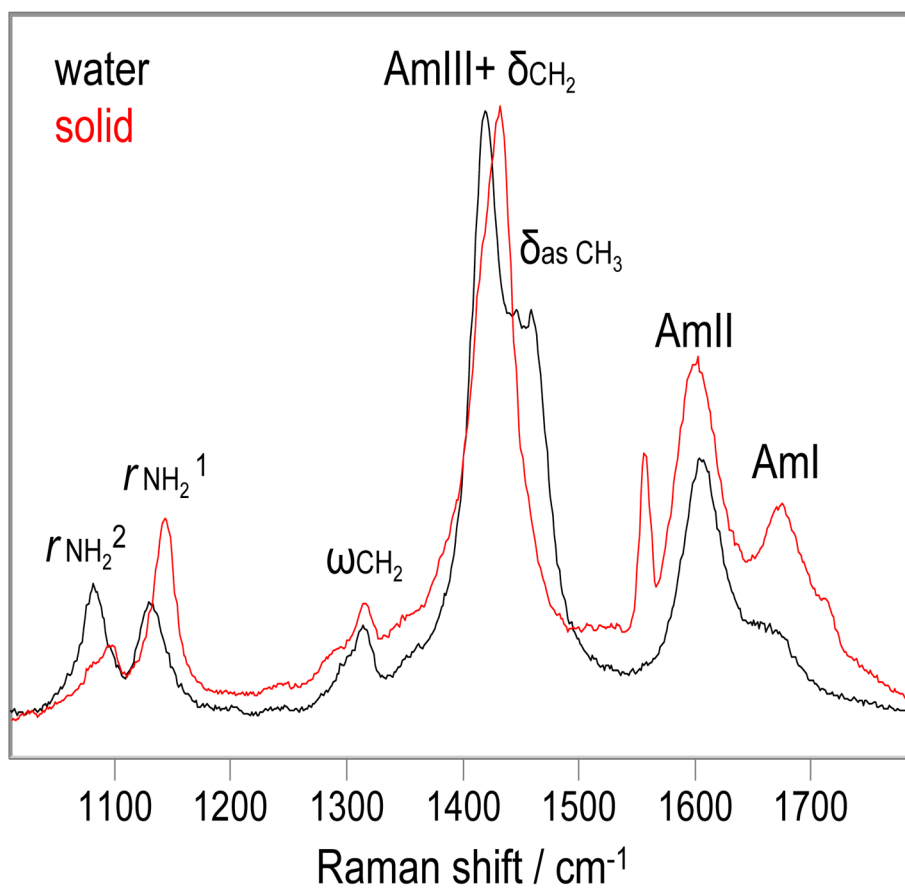


**Figure 3.** The 204 nm excited UVRR spectra of valeramide solid (**Red**) and in water (**Black**) at 22 °C. Water contributions were removed. The intensities were normalized to the AmIII+ $\delta$ CH<sub>2</sub> peak height.

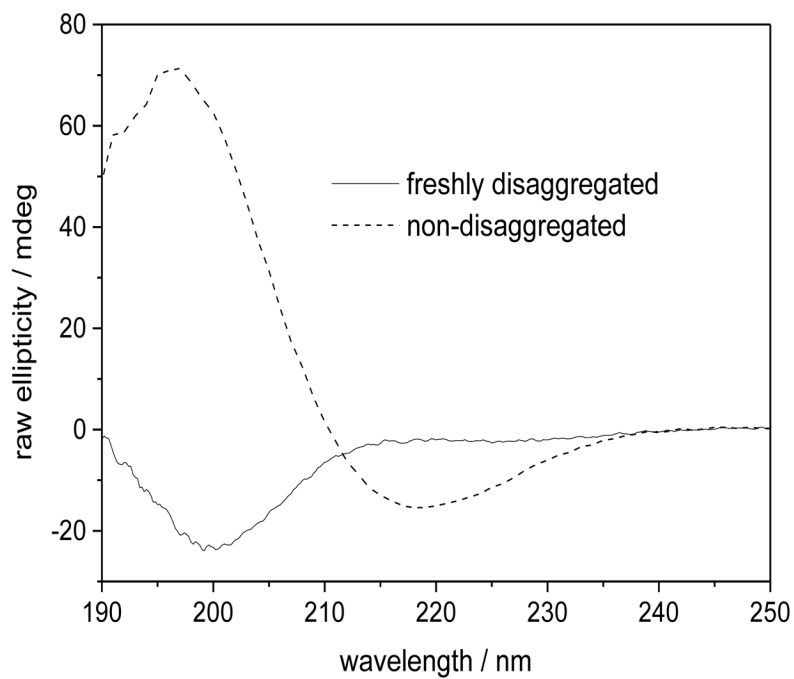


**Figure 4.** CD spectra of 1 mg/ml DQ10 (solid line) and NDQ10 (dashed line) in pure water at 22 °C. Measured by using a 0.02 cm path length cuvette.

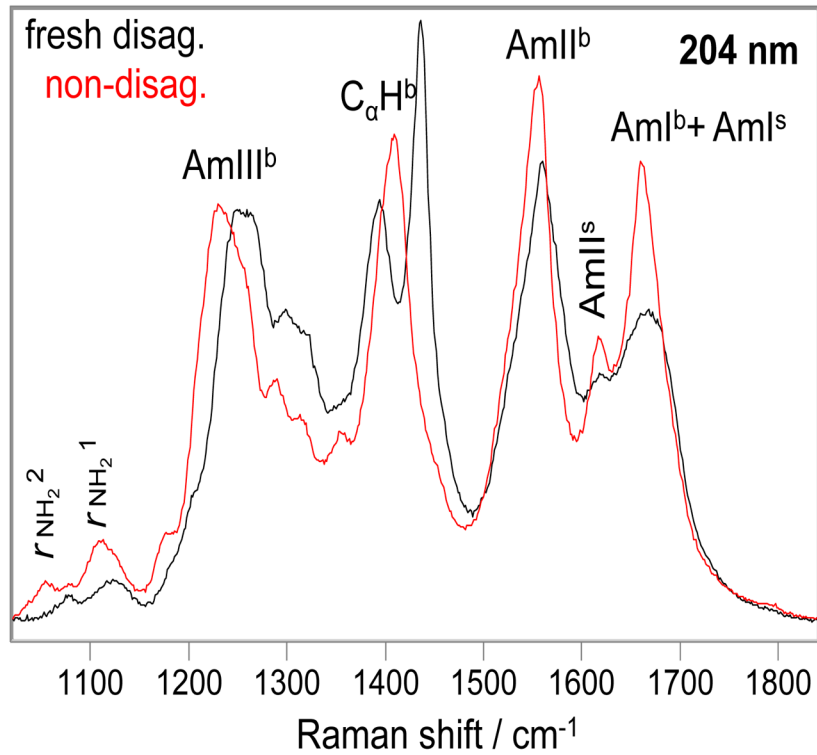


**Figure 5.** The 204 nm excited UVRR spectra of the DQ10 (**black**) and NDQ10 (**red**) in pure water at 22 °C. <sup>b</sup> indicates backbone vibration; <sup>s</sup> indicates side chain vibration. The intensities were normalized to the AmIII<sup>b</sup> peak height.

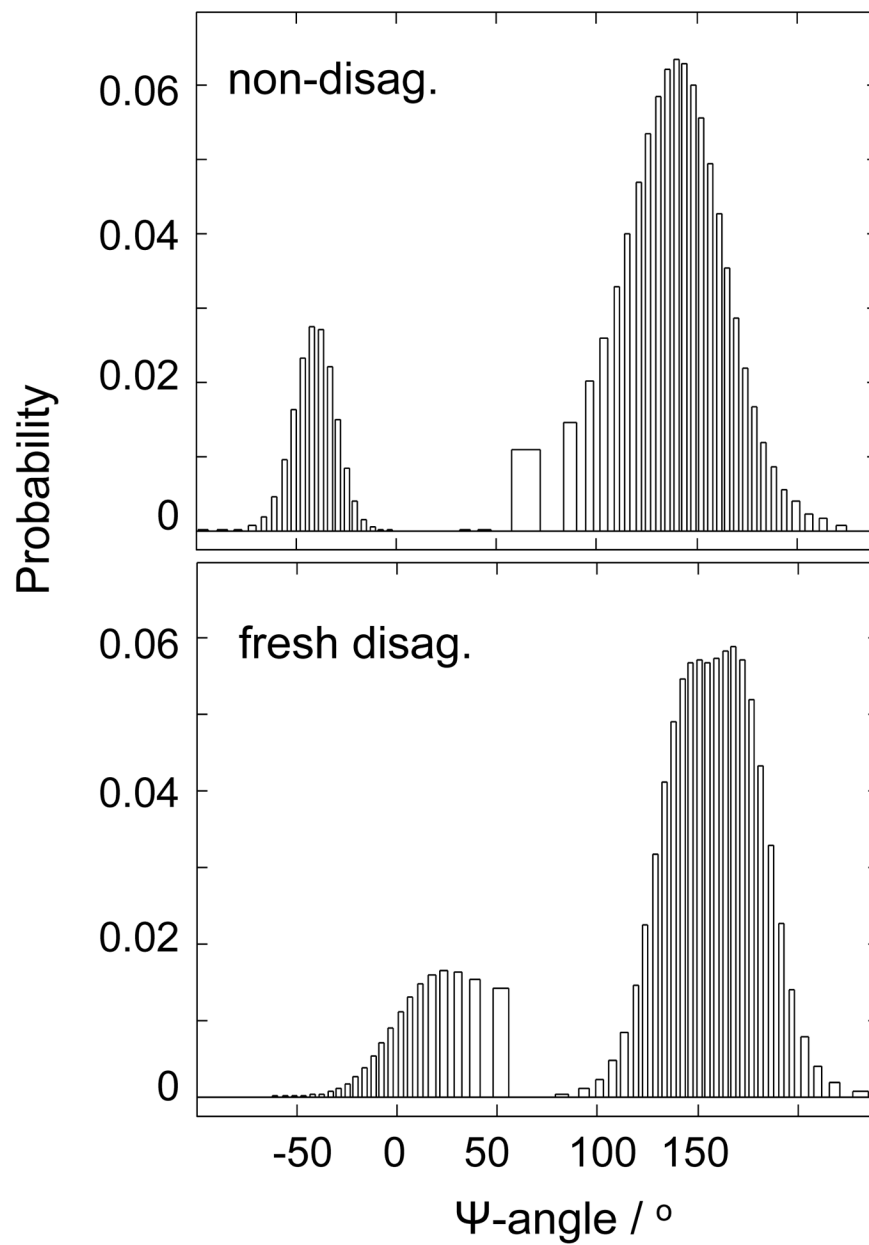


**Figure 6.** Calculated  $\Psi$ -angle distributions for the NDQ10 and DQ10 in pure water at 22 °C.

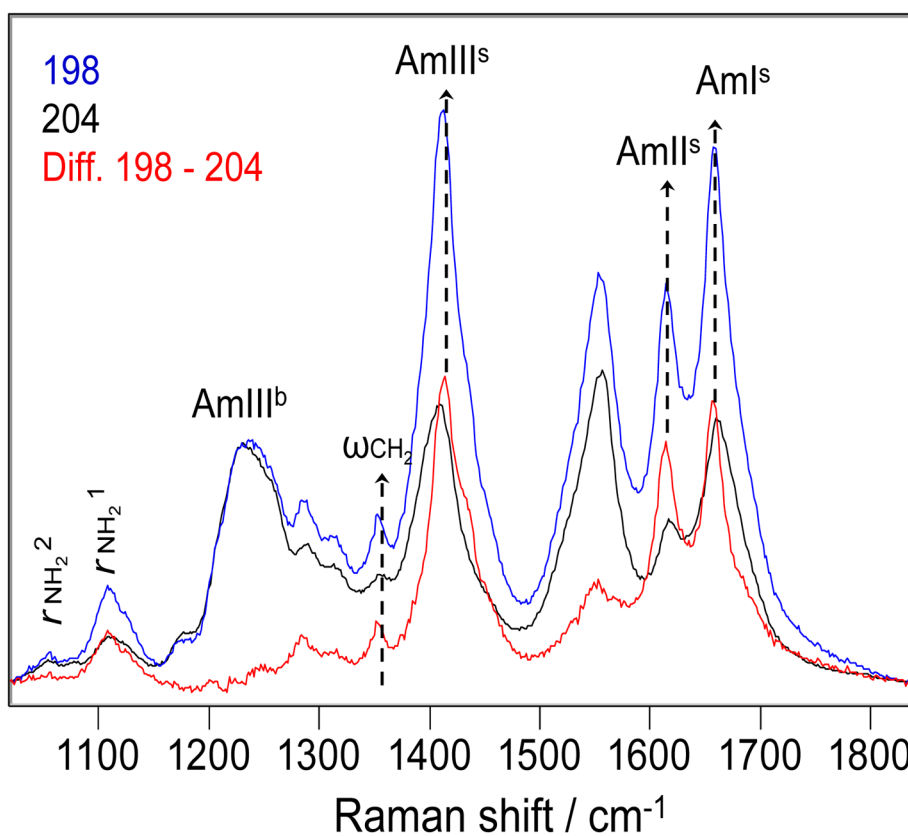


**Figure 7.** The 198 (blue) and 204 nm (black) excited UVRR spectra of the NDQ10 in pure water at 22 °C, and the difference spectrum between them (red). The intensities were normalized to the AmIII<sup>b</sup> peak height before spectral subtraction.

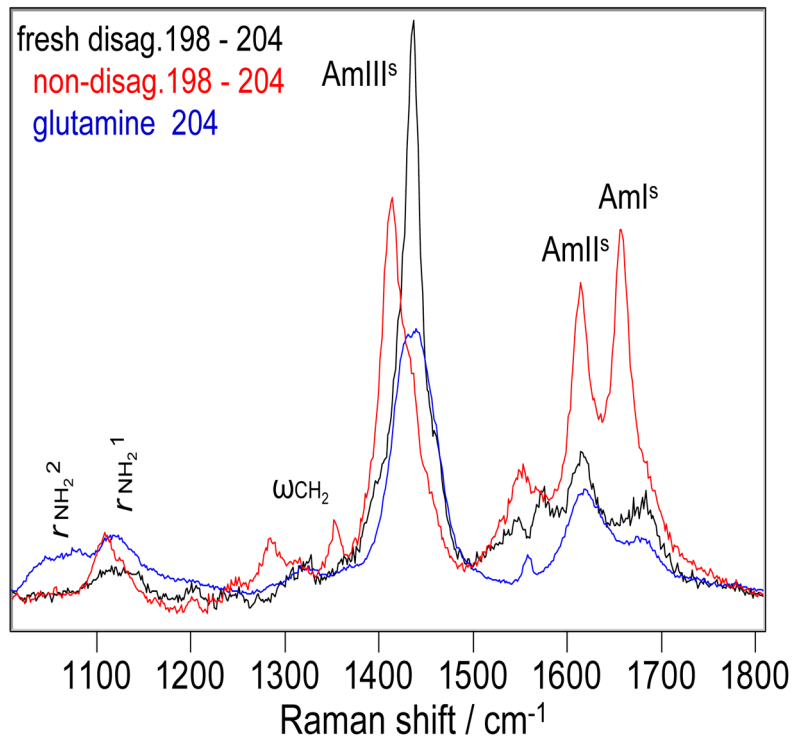


**Figure 8.** The difference spectra between the 198 and 204 nm excited UVRR spectra of the NDQ10 (**red**) and DQ10 (**black**) in pure water at 22 °C. The 204 nm excited UVRR spectrum of glutamine in pure water at pH 1.6 at 22 °C (**blue**).

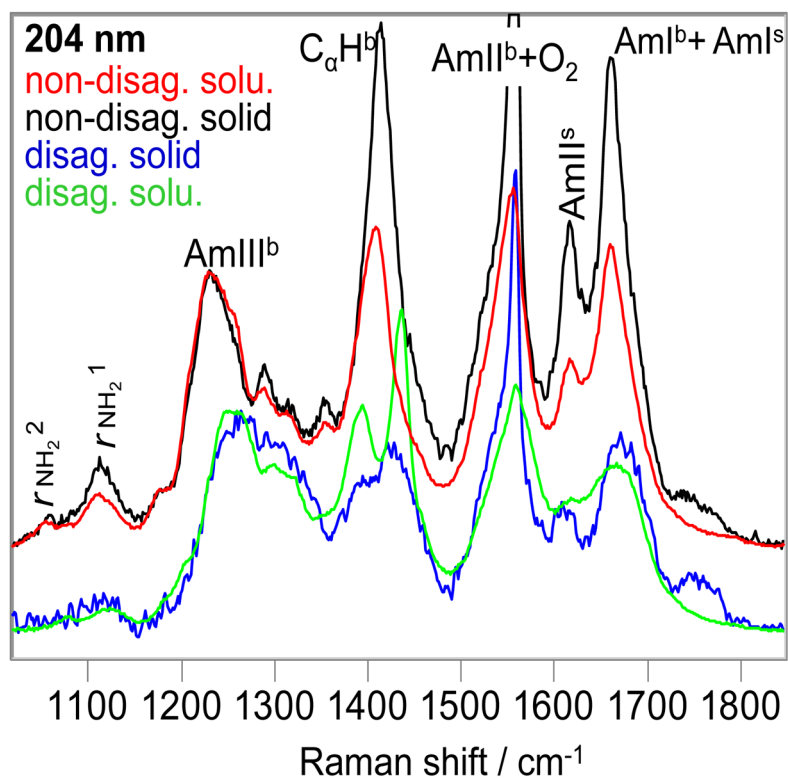


**Figure 9.** The 204 nm excited UVRR spectra of the NDQ10 solid (**black**) and solution (**red**), DQ10 solid (**blue**) and solution (**green**) at 22 °C. <sup>b</sup> indicates backbone vibration; <sup>s</sup> indicates side chain vibration. The intensities were normalized to the AmIII<sup>b</sup> peak height.

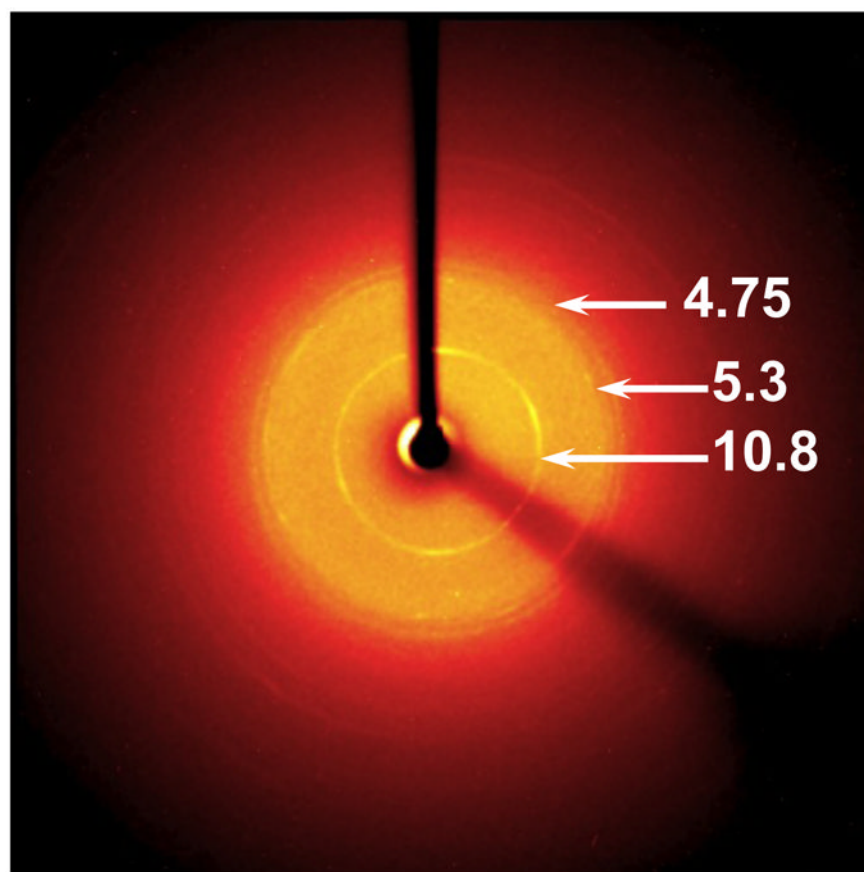


**Figure 10.** Powder x ray diffraction of NDQ10 solid. The sample was prepared by slowly evaporating NDQ10 solution on a glass slide over ~ 2 days.

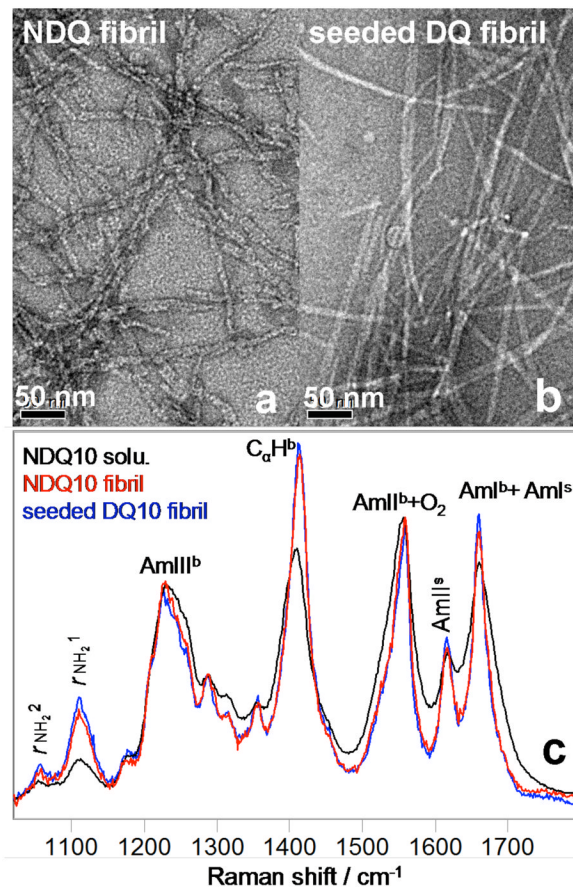


**Figure 11.** Electron micrographs of (a) NDQ10 fibrils in pure water after incubation at 60 °C for ~ 1 week and (b) DQ10 fibrils in pure water upon seeding with 2% NDQ10 solution after incubation at 60 °C for ~ 4 days. (c) 204 nm excited UVRR spectra of the NDQ10 fibrils, the DQ10 fibrils and the NDQ10 solution at 22 °C.

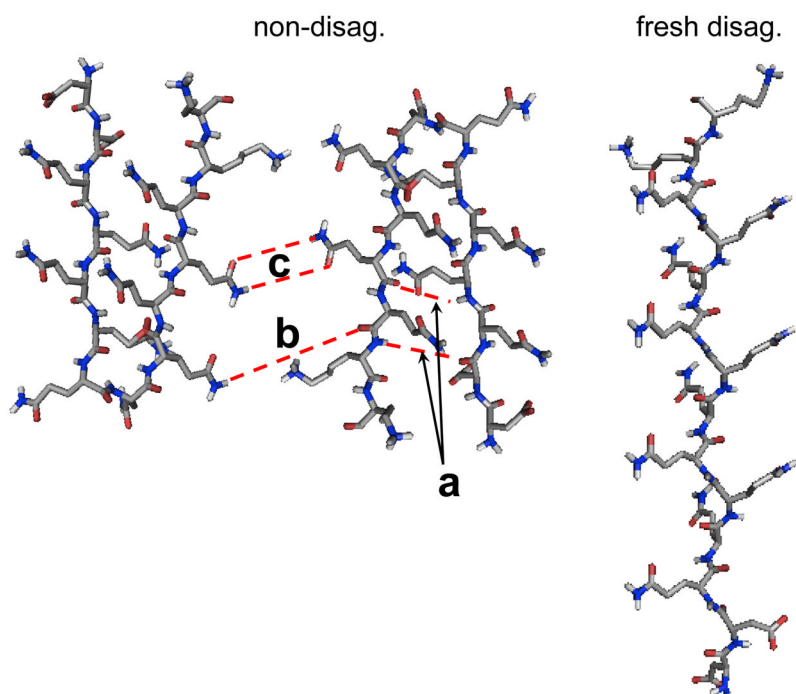


**Figure 12.** Proposed structures of NDQ10 and DQ10. NDQ10 occurs as  $\beta$ -sheets in which the GLN side chains form HB to the backbone or other GLN side chains. DQ10 adopts PPII and 2.5<sub>1</sub>-helix conformations in which the GLN side chains form HB to water. Main chain – main chain HB **a**, main chain – side chain HB **b**, side chain – side chain HB **c**.

**Table 1**

The measured total differential Raman cross sections for valeramide (mbarn·molecule<sup>-1</sup>·sr<sup>-1</sup>) at 22 °C.

	$\Delta_{\text{ml}}$	$\Delta_{\text{mlII}}$	$\delta_{\text{asCH}_3}$	$\Delta_{\text{mlII}} + \delta_{\text{CH}_2}$	$\omega_{\text{CH}_2}$	$r_{\text{NH}_2}^1$	$r_{\text{NH}_2}^2$
vex = 204 nm	in water	5.4	17	21	33	3.3	5.0
	in acetonitrile	11	3.1	13	29	3.2	1.7
vex = 198 nm	in water	14	52	58	94	11	14
	in acetonitrile	41	50	35	91	10	12

\* We did not calculate the Raman cross sections for valeramide powder because of the lack of an intensity internal standard.

**Table 2**

The measured AmI, AmII, rNH<sub>2</sub><sup>1</sup> and rNH<sub>2</sub><sup>2</sup> frequencies of valeramide.

	AmI/cm <sup>-1</sup>	AmII/cm <sup>-1</sup>	rNH <sub>2</sub> <sup>1</sup> /cm <sup>-1</sup>	rNH <sub>2</sub> <sup>2</sup> /cm <sup>-1</sup>
in water at 22 °C	1666	1606	1132	1082
in water at 65 °C	1666	1608	1130	1080
in acetonitrile at 22 °C	1687	1617	1126	1066
solid at 22 °C	1676	1601	1142	1090